Assessing the Role of Soil Moisture in Stomatal and Non-Stomatal Ozone Uptake Across Seasons

Authors: Vladislavs Šingarjovs

Supervisors: Laurens Ganzeveld, Michiel van der Molen

Meteorology and Air Quality Group, Wageningen University

08/04/2025

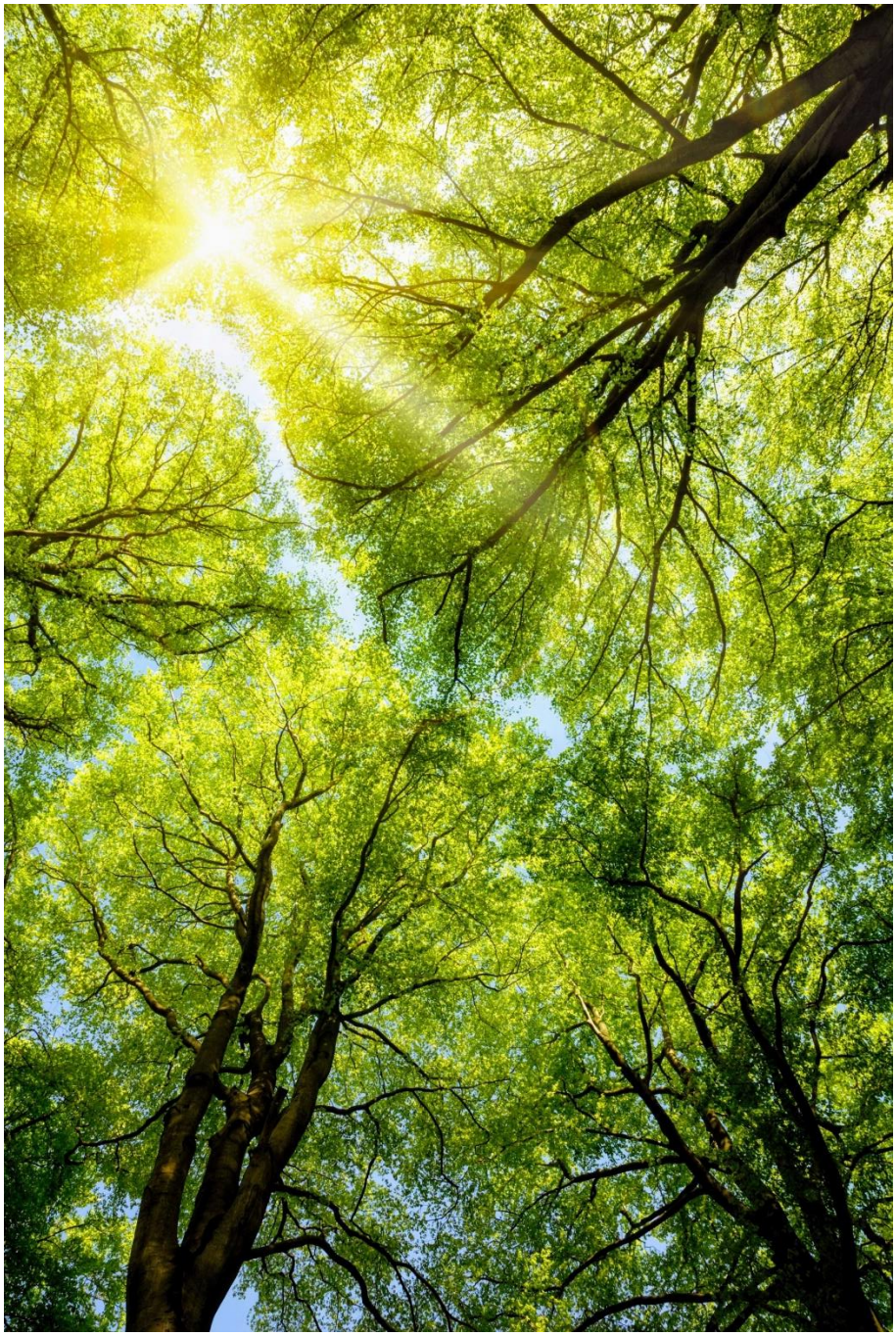

Earth.com. (n.d.). [Photograph of forest canopy with sunlight]. In Complex canopies help forests recover from disturbances. Retrieved February 21, 2025, from https://www.earth.com/news/complex-canopies-help-forests-recover-from-disturbances/

Contents

1. Abstract

This study investigates how soil moisture influences ozone uptake in forest canopies via both stomatal and non-stomatal mechanisms. At Borden Forest in Ontario, field measurements and model simulations were used to assess the impact of soil moisture, measured at two depths (2 cm and 50 cm), on plant water stress and gas exchange including stomatal uptake. The analysis shows that deeper soil layers provide a more stable water supply, effectively capturing the limitations on stomatal uptake during water deficit conditions. An assessment of effective soil moisture indicates that the water controlling stomatal opening appears predominantly found at an estimated depth of about 162 cm, suggesting that conventional shallow measurements may miss critical subsurface water reserves. Simulations using the Multi-Layer Canopy and CHemistry Exchange Model (MLC-CHEM) that incorporated deeper soil moisture estimates based on the observed long-term weekly optimum and the actual stomatal conductance improved the simulated ozone deposition velocity (V_{dO3}) estimates by approximately 32–38% in magnitude and reduced interannual variability errors by roughly 14–18%, particularly during mid-to-late summer when moisture stress is most pronounced. However, under high relative humidity, the model continued to underestimate V_{dO3}, showing that additional non-stomatal mechanisms, such as canopy wetness, seem to play a critical role in ozone removal. These findings highlight the necessity of using depth-resolved soil moisture data and fine-tuning parameterizations for both stomatal and non-stomatal ozone uptake for a realistic representation of ozone deposition air quality models.

2. Introduction

Ozone (O_3) is an essential trace gas with two distinct functions in the atmosphere. In the stratosphere, O_3 is crucial for absorbing ultraviolet (UV) radiation protecting terrestrial life from excessive UV exposure (Kampa & Castanas, 2008; IPCC, 2021). In contrast, tropospheric O_3 is regarded as a significant pollutant that is mostly produced by photochemical reactions between nitrogen oxides (NO_x) and volatile organic compounds (VOCs) when exposed to sunlight (Monks, 2005). Enhanced tropospheric O_3 levels impact vegetation functioning (Ashmore, 2005) but also contributes to respiratory and cardiovascular issues (Kampa & Castanas, 2008). Tropospheric ozone also affects climate (Zhou et al., 2017) being a greenhouse gas but also impacts climate indirectly through increasing CO_2 concentrations due to the induced vegetation damage and resulting decrease in photosynthesis (Sitch et al., 2008)

Dry deposition is one of the main pathways for O_3 removal from the troposphere including both stomatal and non-stomatal removal for vegetated surfaces. The efficiency of this removal of O_3 by dry deposition is expressed by the dry deposition velocity (V_{dO3}), calculated as the observed dry deposition flux normalized with the surface layer concentration (C_{surf}). Models actually rely on prescribing or calculating this vegetation dry deposition velocity, using stomatal and non-stomatal uptake models and parameterizations, to simulate the dry deposition flux as $V_{dO3} \times C_{surf}$.

Stomatal uptake occurs when O_3 is taken up by the plant leaves through the stomata, whereas non-stomatal uptake refers to O_3 absorption at external surfaces, such as leaf cuticles, bark, and soil (Clifton et al., 2023; Visser et al., 2021; Anav et al., 2018). Notably, by allowing direct contact between O_3 and internal physiological processes, the stomatal uptake can induce the O_3 related plant damage. (Davison & Barnes, 1998). Increased levels of O_3 inside leaf tissues may lead to oxidative stress, decreased photosynthetic efficiency, and limited growth (Ashmore, 2005; Davison & Barnes, 1998).

Recent studies highlight the key role of soil moisture (SM) in influencing both stomatal and non-stomatal uptake. O_3 diffusion into leaves is enhanced by a sufficient amount of SM, which supports stomata to open for gas exchange (including transpiration and CO_2 assimilation) (Anav et al., 2018; Visser et al., 2022). Simultaneously, high SM changes canopy microclimate by increasing local relative humidity (RH), thus increasing formation of wet surfaces, which increase

non-stomatal O_3 uptake (Clifton et al., 2023). This phenomenon is especially visible at night or during periods of high RH when leaf surfaces remain wet, supporting additional O_3 removal from the atmosphere (Visser et al., 2021; Zhou et al., 2017). Conversely, water-limited environments suppress stomatal opening, reduce canopy wetness, and limit both stomatal and non-stomatal O_3 uptake (Visser et al., 2022; Anav et al., 2018).

Despite the recognition that SM significantly controls O_3 deposition, remaining knowledge gaps include the role of soil moisture present at different depths, the influence of seasonal dynamics, and the interaction with other environmental factors such as humidity, temperature, canopy wetness, VOC emissions, and NO_x concentrations (Anav et al., 2018; Visser et al., 2022; Clifton et al., 2023). According to observations from semi-arid and boreal ecosystems, deep soil moisture can support plant transpiration and stomatal conductance (g_s) even when surface layers are dry and, consequently, affecting the O_3 flux in ways not captured by shallow soil measurements alone (Anav et al., 2018). However, it is still not fully understood how seasonal changes—such as variations in temperature, precipitation patterns, and phenological cycles—might affect the balance between stomatal and non-stomatal O_3 uptake (Visser et al., 2021). Moreover, environmental drivers like humidity, temperature, and leaf wetness can support increased non-stomatal uptake, whereas increased concentrations of VOCs and NO_x, i.e. due to enhanced emissions for dry and warm conditions, can influence the role of chemical reactions involving O_3 near the surface (Zhou et al., 2017).

In addition to these recognized knowledge gaps, the temporal variability of SM at different depths may provide useful insights into their involvement in modulating stomatal conductance and O_3 uptake. Specifically, soil moisture stress (F_{ws}) is determined by more than only the absolute SM level relative to the critical thresholds (W_{cr} and W_p), which in turn impacts stomatal conductance (g_s) and V_{dO3}. Instead, differences in the level and temporal variability of sub-surface (~ few cm) and deeper (~ 0.5m) soil moisture measurements may result in different temporal patterns in g_s. These differences in the temporal dynamics of SM stress may alter the biases between observed and simulated V_{dO3} (primarily driven by g_s), suggesting whether deeper SM has a greater influence over stomatal processes than shallower SM. Analysing the temporal variability in the bias between observed and modelled V_{dO3} and g_s can help identify the effective depth of SM controlling stomatal and O_3 deposition processes, addressing a critical uncertainty identified in recent studies (Visser et al., 2021; Clifton et al., 2023; Anav et al., 2018).

Accurate, high-temporal-resolution measurements of O_3 fluxes are essential for revealing the temporal dynamics of stomatal and non-stomatal uptake. These measurements allow to distinguish how O_3 fluxes respond to changing environmental conditions, such as shifts in soil moisture or canopy wetness, on diurnal to seasonal timescales (Clifton et al., 2023; Visser et al., 2021). Without high temporal resolution data, it is difficult to determine the timing, magnitude, and relative contributions of stomatal and non-stomatal sinks, resulting in uncertainties in process-level understanding and model parameterization (Zhou et al., 2017). Building on these empirical findings, recent modeling approaches aim to optimally represent the role of both plant-physiological and (biogeo-) chemical processes in O_3 dry deposition models.

One of those models to improve the representation of these processes is the Multi-Layer Canopy and CHemistry Exchange Model (MLC-CHEM). This model has been applied to represent the processes involved in atmosphere-biosphere exchange of reactive compounds and aerosols, both in so-called online approaches, being coupled with large-scale chemistry and transport models, or in an offline set-up being constrained with observed field measurements. The model calculates the vegetation canopy-scale V_{dO3} from the simulated canopy-top flux and C_{surf} for comparison with the observed flux-based V_{dO3}. MLC-CHEM simulates for each canopy layer the leaf-scale stomatal conductance (g_s) and CO_2 and other trace gas fluxes using an assimilation-stomatal conductance model (A-g_s). A-g_s accounts for key differences between C_3 and C_4 photosynthesis, where C_3 plants fix CO_2 into a three-carbon compound (3-PGA), while C_4 plants fix CO_2 into a four-carbon compound (oxaloacetate). This results in different water use efficiencies

and responses to environmental conditions (Visser et al., 2021, 2022). In practice, however, A-g_s may overestimate CO_2 fluxes due to the challenge of accurately capturing assimilation efficiency (Ainsworth & Rogers, 2007). By contrast, O_3 flux measurements offer a more direct approach to infer g_s, because once O_3 enters the leaf, the internal pore space acts essentially as a perfect sink, making daytime O_3 deposition velocity (V_{dO3}) a good proxy for g_s—especially under high insolation and non-limiting soil moisture (Anav et al., 2018). Nevertheless, it is also important to note that O_3 uptake partly relies on non-stomatal processes. Investigating the ratio of stomatal O_3 uptake to total O_3 deposition (g_s/V_{dO3}) helps separate the roles of stomatal and non-stomatal pathways (Visser et al., 2021).

Lastly, the non-stomatal O_3 uptake involves complicated interactions with in-canopy chemistry, including the production of biogenic volatile organic compounds (BVOCs) by trees and the emission of NO_x from soil. Both of these can react with O_3 and change its deposition rates. Furthermore, canopy wetness from rainfall and dewfall amplify non-stomatal uptake by increasing leaf surface contact with O_3 (Altimir et al., 2006). To further understand the impact of SM, canopy properties, and atmospheric chemistry on O_3 fluxes, improved modeling approaches, considering the role of in-canopy interactions including emissions, chemistry, deposition and turbulent exchange as included in MLC-CHEM, are needed. Additionally, integrated long-term (multi-year) field measurements covering a wide range of conditions impacting O_3 deposition, are necessary.

In sum, by combining direct long-term O_3 flux measurements with multi-layer canopy models, this thesis aims to assess and highlight the relationship of stomatal and non-stomatal processes under varying moisture regimes, seasons, and environmental drivers. This is done relying on a long-term measurement dataset collected for a mixed forest located in eastern Canada. Previous analysis of the observed and multi-model simulated V_{dO3} at this mixed forest site showed that all models, including MLC-CHEM, being constrained with observed SM substantially underestimated V_{dO3} especially for summer conditions (Clifton et al., 2023). In this context, the following research questions are addressed:

- How representative are sub-surface and deeper soil moisture measurements in reflecting its limiting effect on O_3 uptake?
- Can inclusion of O_3 flux data improve the LE-observation based estimation of canopy-scale stomatal conductance?
- Does incorporating estimates of soil moisture at a deeper level than where soil moisture has been measured, into models improve predictions of stomatal conductance and, consequently, O_3 deposition velocity?

Alongside the research questions, several hypotheses were developed. First, SM measured at 50 cm depth captures the limiting effect better than measurements at 2 cm depth. Second, plants access water at the mixed forest site at even deeper levels than 50 cm and which we can infer from the observed maximum- and actual LE observations, which are used as a proxy for stomatal conductance measurements. Third, incorporating the inferred deeper level SM into dry deposition models will reduce the underestimation of O_3 deposition velocity and improve model accuracy.

Building upon the work of Clifton et al. (2023), Visser et al. (2021, 2022), and Anav et al. (2018), the overarching goal is to advance our understanding of O_3 deposition mechanisms and improve predictions related to air quality, ecosystem health, and climate feedbacks (IPCC, 2021; Monks, 2005).

3. Methodology

To address the research questions and assess the role of soil moisture in regulating ozone uptake, a combination of data analysis and modeling was used. The following section describes the study

site, data and model descriptions, and methods used to quantify stomatal conductance and infer the effective soil moisture levels and depth that controls stomatal exchange and ozone stomatal deposition. Likewise, it describes the soil moisture attenuation function applied to assess the limiting effects of soil moisture on ozone deposition.

3.1. Site and data description

For this research measurements were taken at the Borden Forest Research Station, located near Newmarket, Ontario (44°19′ N, 79°56′ W), Canada. This station is used for atmospheric and forest interaction studies in Canada's air pollution research initiatives and has contributed data to the Air Quality Model Evaluation International Initiative (AQMEII) (Rao et al., 2011). The station is situated in a forest, which is a natural regrowth from farmland abandoned when the base was established around 1916. The Borden Forest is a mixed forest that consists mostly of Red Maple (Acer Rubrum), White Pine (Pinus Strobus), Large-tooth Aspen (Populus Grandidentata), and White Ash (Fraxinus Americana).

The Borden Forest station has a 33 m meteorological tower to conduct measurements throughout the whole year. The tower is equipped with instruments for monitoring meteorological conditions (e.g., air temperature, wind speed, relative humidity) and fluxes, including latent heat (LE), carbon dioxide (CO_2), and O_3. In addition, soil moisture and soil temperature are recorded at the Borden Forest site at two depths (2 cm and 50 cm). A five-year dataset (2008–2013) provides useful temporal coverage for examining contrasting meteorological and biological conditions. Combining O_3 concentration measurements with flux data allows for the calculation of ozone deposition velocity (VdO_3) (Monks, 2005; Clifton et al., 2023). Detailed information on soil properties and piezometer measurements was retrieved from the Government of Canada website, which provides extensive datasets on various soil types and their characteristics. The piezometer data indicate water table fluctuations ranging from 0.25 m to 5.7 m below the surface. The stomatal conductance values used in this study were obtained from the study by Anam et al. (2024)

3.2. Model description

The MLC-CHEM model simulates ozone deposition processes in forests. It accounts for both stomatal and non-stomatal ozone uptake and resolves the vertical structure of the canopy by dividing it into multiple layers (minimum of 2 up to > 10 layers), allowing the vertically-resolved simulation of the impact of the canopy environment of the physical drivers of both stomatal uptakes, which are influenced by plant physiology and SM, and non-stomatal processes that occur on soil, leaves, and other surfaces (Clifton et al., 2023). In this way the model allows to study the role of the vertically resolved partitioning between stomatal and non-stomatal removal of O_3, e.g., as a function of vertically gradients in canopy wetness, photolysis rates and reactant concentrations. Likewise, it is driven by the observed micrometeorological data which includes SM.

The modular design of MLC-CHEM enables extensive studies of canopy-atmosphere interactions across multiple geographic and temporal dimensions. The model includes both a basic two-layer set-up in its coupling to large-scale chemistry and transport models (e.g., Ganzeveld et al., 2010) and more detailed multi-layer configurations that produce high-resolution vertical profiles of tracer concentrations and fluxes in its application for detailed field measurement analysis. It also incorporates a gas-phase chemistry scheme (based on the CBM4 mechanism) to consider the contribution of in-canopy chemical interactions on atmosphere-biosphere exchange fluxes.

3.3. Stomatal conductance

Stomatal uptake, being expressed by the stomatal conductance, g_s which is calculated in this study from the Borden forest observations based on the approach provided in Visser et al., (2021) according to:

$$g_s = \frac{LE\, g_a \gamma}{\Delta(R_n - G) + \rho c_p g_a VPD - LE(\Delta + \gamma)} \quad \text{(eq. 1)}$$

where LE is the latent heat flux (W m^{-2}), g_a is the aerodynamic conductance to water vapor (m s^{-1}), γ is the psychrometric constant (0.4 K^{-1}), Δ is the slope of the saturation vapor pressure curve (kPa °C^{-1}), R_n is net radiation (W m^{-2}), G is the ground heat flux (W m^{-2}), ρ is the air density (kg m^{-3}), c_p is the specific heat of air (1010 J K^{-1}kg^{-1}) and VPD is the vapor pressure deficit (kPa).

g_s represents stomatal conductance to H_2O (cm s^{-1}). To express stomatal conductance for ozone, g_s is adjusted by scaling it according to the diffusivity (D) ratio between ozone and water vapor, as follows:

$$g_{s,O_3} = \frac{D_{O_3}}{D_{H_2O}}\, g_{s,H_2O} = 0.61\, g_{s,H_2O} \quad \text{(eq. 2)}$$

3.4. Soil moisture attenuation function

The soil moisture attenuation function is a mathematical representation used in models to describe how SM availability affects specific biological or physical processes, such as stomatal conductance in plants. The function (F_{ws}) modifies the optimal stomatal conductance dependent on the soil's water content and ranges from 0 to 1, where:

- F_{ws} = 1: No water stress, indicating optimal level of soil moisture for the process (e.g., maximum stomatal conductance).
- F_{ws} < 1: Increasing water stress, resulting in reduced process rate due to insufficient soil moisture levels.
- F_{ws} = 0: Complete water stress, where soil moisture is at or below the permanent wilting point (W_p), and stomatal opening is completely restricted.

F_{ws} is calculated based on soil moisture content (W_s) and two critical thresholds:

- W_p (permanent wilting point): The soil moisture level below which plants cannot extract water, leading to a value of F_{ws} = 0.
- W_{cr} (critical soil moisture): The soil moisture level below which the effects of water stress begin, typically where F_{ws} starts decreasing from 1.

In this study several different F_{ws} functions were analyzed but only the baseline polynomial formula used to calculate F_{ws} is discussed below. In order to see all the other functions, check Discussion and Appendix.

$$F_{ws} = 2 \times \left(\frac{Ws - Wp}{Wcr - Wp}\right) - \left(\frac{Ws - Wp}{Wcr - Wp}\right)^2 \quad \text{(eq. 3)}$$

This polynomial function reflects a gradual decrease in SM and a quick drop near the permanent wilting point (see Figure 1 in Results). Such dimensionless soil-moisture (or water-stress) factors

have been widely used in stomatal conductance and ecosystem productivity models (Jarvis, 1976; Porporato et al., 2001). Although these references may use slightly different functional shapes (piecewise linear, sigmoidal, etc.), the conceptual framework, translating soil water deficits into a multiplicative stress factor, remains consistent across models (Landsberg & Waring, 1997; Granier et al., 2007). Based on soil properties at Borden Forest, W_{cr} and W_p were determined, and corresponding F_{ws} values were calculated for each observed W_s value.

3.5. Soil Properties

The measurements were taken in Borden Forest, which has two major soil types: luvisolic soil, which accounts for around 80% of the soil composition, and organic soil, which makes up the remaining 20%. Luvisolic soils have a loamy or clay-rich texture, whereas organic soils have a peaty texture and are heavy in organic matter, resulting in greater water retention capacity but slower water release rates (Zettl et al., 2011; Famiglietti & Wood, 1994).

To define representative critical soil moisture and permanent wilting point thresholds for the site, typical W_{cr} and W_p values for both Luvisolic and Organic soils (as percentages of field capacity, FC) were obtained from literature (Table 1).

Table 1: Critical soil moisture and permanent wilting point percentages of the field capacity for Luvisolic and Organic soil types.

Soil type	**W_{cr} (% of FC)**	**W_p (% of FC)**
Luvisolic	~0.75	~0.35
Organic	~0.80	~0.20

Weighted averages of W_{cr} and W_p for the overall soil composition at Borden Forest were then calculated using the fixed ratios (80% Luvisolic and 20% Organic) to arrive at value of 0.76 for W_{cr} and 0.32 for W_p.

Site-specific values of field capacity (FC) at two measurement depths (2 cm and 50 cm) were determined directly from observed maximum SM data collected over a prolonged wet period, assuming these values closely represent FC at respective depths (following methods described by Feddes et al., 2001; Oke, 2002). Subsequently, these depth-specific FC values were multiplied by the site-weighted fractions of W_{cr} and W_p (0.76 and 0.32, respectively), yielding the corresponding W_{cr} and W_p values for each depth. Finally, the soil moisture attenuation function (F_{ws}) was applied to assess how soil moisture stress changes with moisture content at each depth (2 and 50 cm).

3.6. Data filtering

A set of filters was established to exclude unsuitable data for analyzing the impact of SM limitations on stomatal conductance and O_3 deposition. Data were excluded from the multi-year Borden dataset according the following criteria:

1. Precipitation events: All data during precipitation events were removed because rainfall can wet the canopy and influence stomatal behavior by temporarily overriding soil moisture limitations. Wet canopies cause stomatal closure and higher boundary-layer resistance, reducing the accuracy of g_s measurements (Jarvis & McNaughton, 1986; Oishi et al., 2008).

2. Leaf Area Index (LAI) < 1: Data points with LAI smaller than 1 were excluded due to insufficient canopy coverage for meaningful stomatal conductance study (Bréda et al., 1995).

3. Shortwave incoming solar radiation (SW_{in}) < 100 W m^{-2}: Only daytime stomatal conductance measurements for SW_{in} > 100 W m^{-2} have been applied to also exclude early morning or late evening, when stomatal conductance is small due to decreased photosynthetic demand (Damour et al., 2010).

4. Relative humidity (RH) > 90%: Data points with RH higher than 90% were removed, due to the possibility of dew formation and canopy wetting at this level of RH. Wet canopies can reduce stomatal conductance by lowering vapor pressure deficits (Monteith & Unsworth, 2008). In an additional analysis on the effect of canopy wetness on O_3 uptake this criterion was removed.

5. 0 cm s^{-1} < g_s < 2 cm s^{-1}: observations-inferred g_s values lower than 0 cm s^{-1} were removed from the analysis, since they are physically impossible and likely represent measurement errors. In addition, inferred g_s values greater 2 cm s^{-1} were considered outliers, as stomatal conductance rarely exceeds this value in the field. Such high values could result from instrumentation noise or environmental anomalies (Pataki & Oren, 2003).

3.7. Inferred and optimal stomatal conductance

After applying the data filters described in the previous section, two forms of stomatal conductance were calculated: inferred stomatal conductance corrected for soil moisture limitation ($g_{s,Fws}$) and optimal stomatal conductance ($g_{s,opt}$).

First, stomatal conductance derived directly from the observations inherently reflects the actual environmental conditions, including limitations due to SM availability. To quantify explicitly the role of reduced SM in limiting stomatal opening, the observed stomatal conductance values ($g_{s,obs}$) were divided by the F_{ws} calculated from the measured SM at 2 and 50cm :

$$g_{s,Fws} = \frac{g_{s,obs}}{F_{ws}} \quad \text{(eq. 4)}$$

This approach adjusts the $g_{s,obs}$ by effectively removing the estimated influence of SM limitations, resulting in $g_{s,Fws}$ values that approximate stomatal conductance under conditions without soil moisture stress at each measurement depth. Comparing $g_{s,Fws}$ with the original observed stomatal conductance ($g_{s,obs}$) provides insights into the degree to which measured SM at 2 cm and 50 cm depths accurately captures SM limitations. Statistical analyses were conducted to quantify these differences, including metrics such as the t-statistic, p-value, mean absolute error (MAE), root mean squared error (RMSE) and correlation heatmaps between $g_{s,obs}$ and $g_{s,Fws}$ at both depths.

Optimal stomatal conductance ($g_{s,opt}$) represents stomatal conductance under conditions that are optimal in terms of incoming radiation, temperature, and atmospheric moisture, assumed to be unaffected by SM limitations. To derive $g_{s,opt}$, the highest $g_{s,obs}$ values within each calendar week across the entire multi-year measurement period (2008–2013) were first identified. Subsequently, the median of these weekly maxima was calculated for each calendar week, producing a multi-year weekly median maximum stomatal conductance. These weekly median maximum values represent conditions under which stomatal conductance is least likely to be limited by SM, radiation, temperature, or atmospheric moisture stress. In the followed approach, we assume that deviations between the weekly median maximum stomatal conductance ($g_{s,opt}$) and the actual observed weekly mean stomatal conductance ($g_{s,obs}$) primarily reflect SM limitations. This method ensures that the derived $g_{s,opt}$ values capture the maximum potential ozone uptake achievable in the absence of soil moisture stress.

3.8. Effective soil moisture and its depth

To further investigate the SM levels that limit stomatal conductance, as being observed at the Borden mixed forest site, the concept of "effective soil moisture" is introduced. The full derivation for calculating effective soil moisture from $g_{s,obs}$ and $g_{s,opt}$ (via F_{ws}) can be found in the Appendix. In brief, assuming that the F_{ws} represents the impact of reduced SM on stomatal conductance realistically, once F_{ws} is computed by comparing the weekly-mean measured and multi-year weekly optimal stomatal conductance, the soil moisture content (W_s) that corresponds to this F_{ws} is determined. This value is referred to as the effective soil moisture.

Since it is unclear at what depth effective soil moisture values are located, but hypothesized to be located deeper than the measurement depth of 50 cm, two sets of soil properties were tested to calculate it. The first set was based on soil properties characteristic of layers located at a depth of 100 cm. The second set used soil properties of layers located at depths around 50 cm, in case our hypothesis is incorrect. To help determine the necessary soil properties, Figure 12 (see Appendix) and data from the Canadian Soil Landscape Datasets were used.

To estimate the "effective soil moisture" depth, where the present soil moisture should be mostly dominating the impact on vegetation functioning, the SM data need to be normalized. Normalization allows us to express SM values in a standardized way, relative to the soil's ability to retain water. The normalization equation is as follows:

$$W_{s,norm} = \frac{W_s - W_p}{W_{FC} - W_p} \quad \text{(eq. 5)}$$

where $W_{s,norm}$ is normalized soil moisture ($m^3\ m^{-3}$) and W_{FC} stands for the soil moisture at field capacity ($m^3\ m^{-3}$).

It ensures that the effective soil moisture values are interpreted in relation to the SM at wilting point and field capacity, which define the limits of soil water availability. It transforms the SM values into a relative scale from 0, which means the soil is at wilting point, to 1, which means the soil is at field capacity. Additionally, values below 0 indicate extreme drought conditions, whereas values above 1 indicate excess water, that can suggest that the SM value is located within the water table. This normalization, is consistent with methods used in soil physics (van Genuchten, 1980) and ecohydrological modeling (Porporato et al., 2001; Dickinson et al., 1993), allowing for comparisons of soil moisture availability across different depths and soil types.

Next, effective soil moisture depths were approximated by linear extrapolation using the normalized soil moisture values measured at 2 cm and 50 cm depths. Because normalized soil moisture values at 50 cm depth were consistently higher than those at 2 cm, and effective soil moisture values can fell outside this range, extrapolation was necessary to estimate the depth at which the effective soil moisture predominantly occurs.

These extrapolated values will provide the approximate values for the depth where the effective soil moisture is mostly present. This will be compared with the rooting depths of the key tree species and water table measurements at the Borden Forest to assess if this inferred depth can be reconciled with other empirical site information on soil hydrology and vegetation functioning and properties.

To provide a representative overview of SM impacts on stomatal conductance, the effective soil moisture values presented in results section were averaged across multiple soil moisture attenuation functions (see Discussion and Appendix). This averaging approach was chosen due to uncertainties regarding the most suitable F_{ws} formulation for the Borden Forest site, acknowledging that each function has distinct sensitivities to SM.

3.9. Model outputs

After determining the effective soil moisture value, it will be used as input parameter for the MLC-CHEM model simulations. The V_{dO_3} values from these output files will then be analyzed. The default model output, which used the 50cm SM measurements for the multi-model intercomparison (Clifton et al. 2023), will be compared with the output that use the identified effective soil moisture (modified model output) against the V_{dO_3} measurements for the whole day and the 90th percentile, which only captures extreme events.

Then, we will calculate the difference between the default and modified simulations of V_{dO3}, in order to use them to investigate whether a set of meteorological variables has an effect, using the absolute standardized coefficient. This approach will allow us to analyze the magnitude and temporal variability of V_{dO_3} from different model outputs. Likewise, we aim to analyze the relative effect of the selected meteorological variables on biases in V_{dO_3} also to further diagnose the potential role of non-stomatal O_3 uptake mechanisms that might explain these remaining biases.

Finally, we will present the results of some additional sensitivity experiments regarding the representation of non-stomatal removal mechanisms indicated by meteorological variables with the largest role in explaining the remaining biases in V_{dO_3}.

4. Results

Building upon the methodologies described, the results section presents key findings on the relationship between SM, stomatal conductance, and ozone uptake. This includes analyses of soil properties, the influence of SM stress, and comparisons between measured and modeled data to evaluate the validity of the proposed approach on application of the observed and simulated g_s and soil moisture attenuation functions to infer the effective soil moisture levels and depth determining stomatal exchange and O_3 deposition.

4.1. Soil moisture stress at different depths

Calculated values for field capacity (FC), critical soil moisture (W_{cr}), and permanent wilting point (W_p) at depths of 2 cm and 50 cm are presented in Table 2.

Table 2: Field capacity, critical soil moisture and permanent wilting point values for 2 and 50 cm depth.

Depth (cm)	FC (m^3 m^{-3})	W_{cr} (m^3 m^{-3})	W_p (m^3 m^{-3})
2	0.281	0.213	0.089
50	0.194	0.147	0.062

Applying these calculated soil properties to the soil moisture attenuation function resulted in distinct soil moisture stress (F_{ws}) responses at each depth (Figure 1).

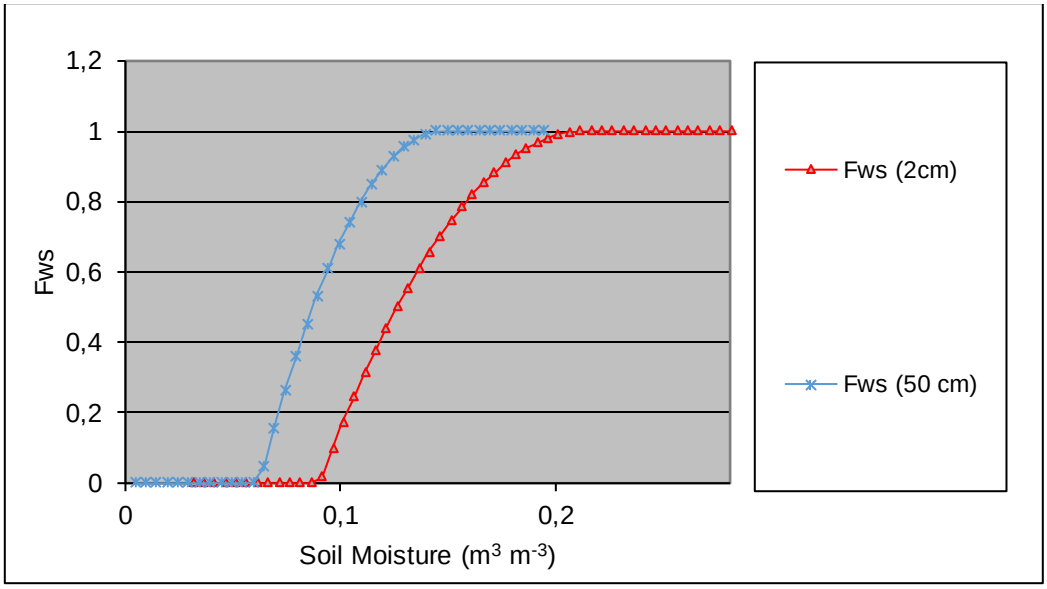

Figure 1: Soil moisture stress function as a function of the measured soil moisture at for 2 and 50 cm depth.

Significant differences were observed between the F_{ws} curves at 2 cm and 50 cm depths. The upper soil layer (2 cm) exhibited overall higher moisture values compared to the deeper layer (50 cm), which can be explained by the presence of more organic matter in the upper soil layers (Baldocchi et al., 2004; Lawrence & Slater, 2008). Organic material enhances the soil's capacity to retain water and release it slowly, thus contributing to higher SM content and a more gradual transition from no stress (F_{ws} = 1) to severe stress (F_{ws} = 0). In contrast, at 50 cm depth, lower organic content and higher mineral fraction likely result in a faster drainage and lower SM values, leading to a more rapid decline in F_{ws} as moisture decreases.

Thus, the transition from non-stress to moisture-limited conditions occurs at higher moisture levels at 2 cm depth than at 50 cm depth, and the decrease in F_{ws} at 2 cm depth is more gradual when compared to that calculated at 50 cm depth. This depth-dependent difference highlights the importance of considering vertical heterogeneity of soil properties when assessing soil moisture stress and its implications for stomatal conductance and ozone uptake.

4.2. Comparison of measured and F_{ws} inferred stomatal conductance

Figure 2 shows the difference between $g_{s,obs}$ and the stomatal conductance corrected with the inferred soil moisture attenuation function, $g_{s,Fws}$ as a function of the measured SM at depths of 2 cm and 50 cm. It is visible that $g_{s,Fws}$ values decline significantly after SM drops below W_{cr}. The decrease becomes more pronounced as SM approaches W_p. Below W_p, all $g_{s,Fws}$ values reach zero, indicating that the leaf stomata , when assuming that the F_{ws} function properly represents the SM limitation effect, close entirely under extreme soil moisture limitation. The 50 cm depth soil moisture stress function demonstrates a more gradual decline in $g_{s,Fws}$ compared to that representative for 2 cm depth, which suggests that the deeper layer provides more stable water availability. This difference indicates that SM at 50 cm depth is less variable and enhances the resilience against rapid SM depletion. It is visible that $g_{s,obs}$ at both depths does not follow the same path as $g_{s,Fws}$ indicating that the actually observed LE and inferred stomatal conductance do not support this SM limiting effect Although it seems that both depths show some limiting effect on stomatal conductance, the soil moisture measurements at both depths do not properly capture the soil moisture limitation effect on g_s.

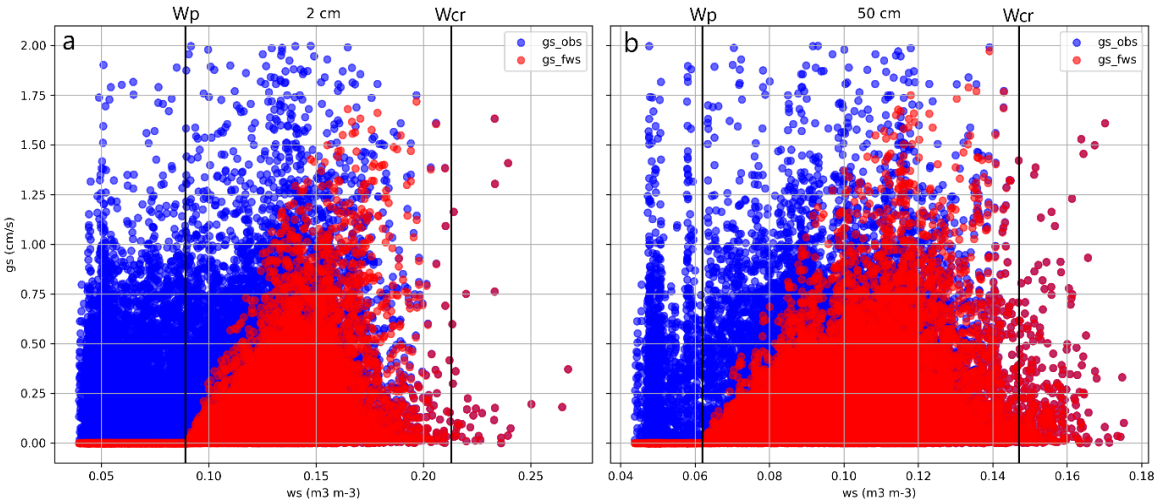

Figure 2: The difference between $g_{s,obs}$ and $g_{s,Fws}$ for soil moisture at depths of 2 (a) and 50 (b) cm.

To quantify the differences between the $g_{s,obs}$ and $g_{s,Fws}$, a statistical analysis was performed for each depth. Table 3 summarizes the t-statistic, p-value, mean absolute error (MAE), and root mean squared error (RMSE).

Table 3: Statistical metrics for stomatal conductance inferred form the soil moisture at 2 and 50 cm depth.

Metric	**2 cm depth**	**50 cm depth**
T-statistic	106.03	82.20
P-value	0	0
MAE	0.178	0.114
RMSE	0.288	0.218

The t-statistics for both depths are exceptionally high, which indicate a statistically significant difference between $g_{s,obs}$ and $g_{s,Fws}$ at both depths. The MAE and RMSE values provide additional support for these results. The MAE is lower using the 50 cm depth SM data (0.114 vs 0.178 at 2 cm depth), indicating a better fit between $g_{s,obs}$ and $g_{s,Fws}$. The RMSE for the 50 cm depth SM data (0.218) is also lower than that using the 2 cm depth SM data (0.288), implying that the g_s inferred using the deeper layer soil moisture data had less deviations between observed and inferred stomatal conductance. Despite the minor difference, it is clear that $g_{s,obs}$ is closer to $g_{s,Fws}$ using the SM measured depth of 50 cm, showing that the SM measurements collected at that depth are better able to capture the limiting effect of SM, although there is still a significant discrepancy especially for the low values of 50cm depth SM measurement.

Correlation analysis depicted in Figure 4 further supports previous results. The correlation coefficient between $g_{s,obs}$ and $g_{s,Fws}$ is 0.71 for the 2 cm depth SM and 0.82 using the 50 cm depth SM. However, at both depths, there is little correlation between stomatal conductance ($g_{s,obs}$ and $g_{s,Fws}$) and SM. This suggests that, despite the strong relationship between $g_{s,obs}$ and $g_{s,Fws}$, SM has little effect on stomatal conductance at these depths.

In summary, the statistical analysis demonstrates that neither depth fully captures the limiting effect of SM on g_s. Compared to the 2 cm depth, the 50 cm depth SM data provide a more accurate representation of the limiting influence of soil moisture on stomatal conductance. Nevertheless, even at 50 cm, the persistent differences between $g_{s,obs}$ and $g_{s,Fws}$ suggest that deeper soil layer measurements are required to fully capture soil moisture's limiting influence on g_s.

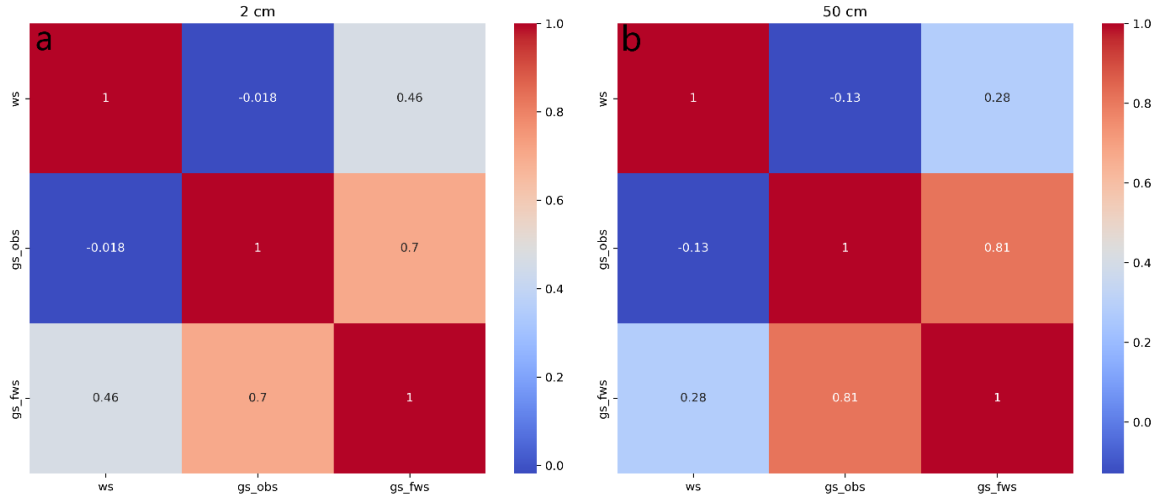

Figure 4: Correlation heatmaps between soil moisture (ws), $g_{s,obs}$ and $g_{s,Fws}$ for 2 (a) and 50 (b) cm depth.

4.3. Optimal stomatal conductance, effective soil moisture and its depth

Figure 5 shows a comparison of weekly $g_{s,obs}$ values with weekly $g_{s,opt}$. To derive $g_{s,opt}$, the highest stomatal conductance values were identified within each calendar week across the multi-year dataset (2008–2013), assuming these weekly maxima represent conditions optimal in terms of incoming radiation, temperature, and atmospheric- and soil moisture. Weekly $g_{s,opt}$ values are consistently higher than $g_{s,obs}$, indicating that observed stomatal conductance frequently experiences limitations, primarily attributed to soil moisture stress. Furthermore, $g_{s,opt}$ shows distinct temporal fluctuations throughout the growing season, reflecting variations in maximum potential stomatal conductance driven by seasonal changes in environmental conditions, such as solar radiation and atmospheric humidity.

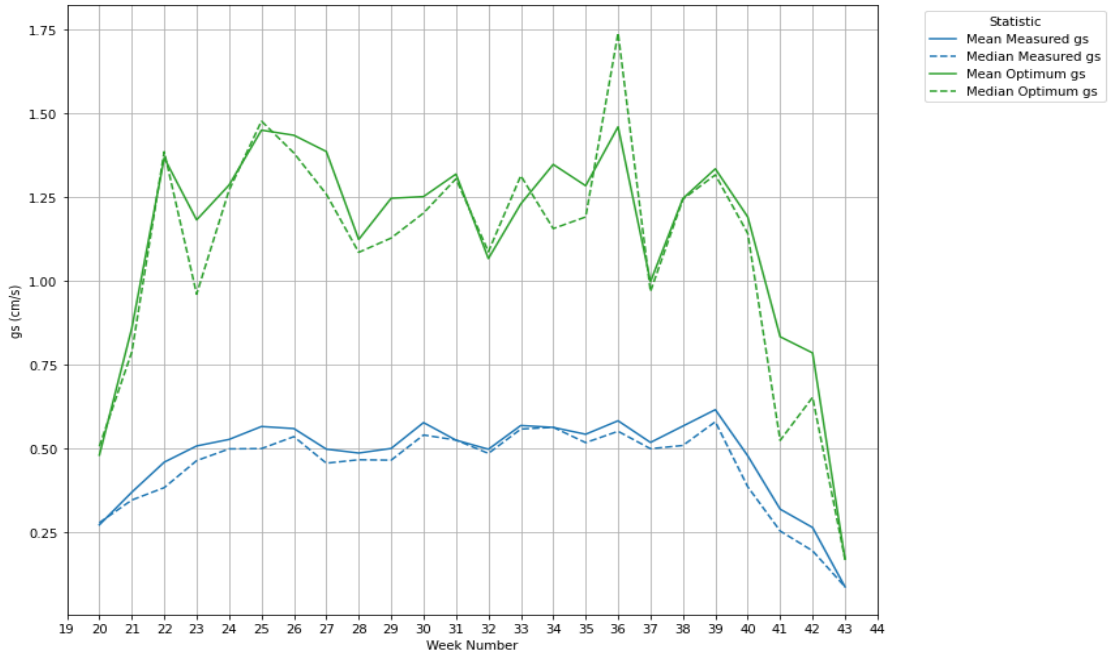

Figure 5: Comparison of weekly measured g_s values with optimal gs values plotted against week number.

Next, effective soil moisture inferred from the $g_{s,opt}$ was evaluated. Figure 6 illustrates the comparison of effective soil moisture values, represented by two sets of soil properties (one derived for soil layers deeper than 100 cm, and another derived for soil layers above 100 cm), alongside measured weekly mean SM values at 2 cm and 50 cm depths. The two different sets of soil properties were chosen because it remains uncertain whether the effective soil moisture controlling stomatal conductance at this site is located near the water table (deeper layers) or within shallower soil layers.

The effective soil moisture calculated using deeper soil properties (at 100 cm depth) is shown as the blue line, while the effective soil moisture calculated using shallower soil properties (at 50 cm depth) is shown as the red line. At both measurement depths, the effective soil moisture values derived from deeper soil properties (blue line) consistently exceed measured SM, implying that this effective moisture likely corresponds to soil layers closer to the water table or at greater depths, where soil moisture levels are generally higher and more constant. In contrast, effective soil moisture estimated using shallower soil properties (red line) often shows values lower than measured SM at both depths, implying that this estimate likely represents moisture levels present in the top ~1m soil profile.

Compared to measured SM at 2 cm and 50 cm, effective soil moisture estimates provide more stable temporal patterns with smaller short-term variations. This reduced variation might mostly reflect a stronger buffering effect of deeper soil layers, which have a higher water holding capacity and are less influenced by temporary climate events impacting the soil moisture reservoir such as precipitation or evapotranspiration (Danie Hillel, 2004). Furthermore, using $g_{s,opt}$ estimated from long-term weekly median maxima reduces short-term variations by smoothing SM estimates. Finally, normalisation of effective soil moisture using soil-specific parameters (field capacity and permanent wilting point) combined with interpolation procedures between measured depths does not only results in enhanced SM levels but also strongly reduces temporal variability compared to the shallow-layer measurements. A next step will be analyzing to what extent these two features of the inferred effective soil moisture impact g_s and V_{dO3}.

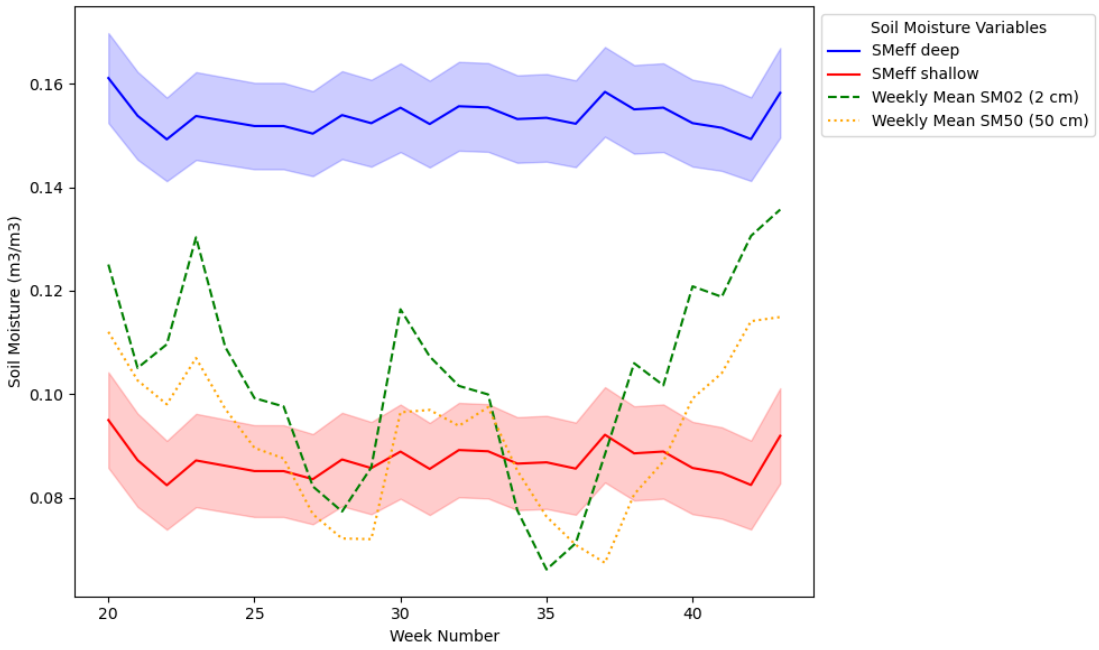

Figure 6: Comparison of weekly effective soil moisture estimated for deeper soil layers (blue line) and shallower soil layers (red line) with weekly mean soil moisture at 2 cm and 50 cm depths (green markers), plotted against the week number.

After normalizing effective soil moisture data together with measured SM at 2 cm and 50 cm, the depth at which effective soil moisture occurs was estimated through interpolation. Using median values from multiple soil moisture attenuation functions (see Discussion and Appendix for details), the approximate median depth where most of this effective soil moisture should be present, was determined to be around 162 cm.

Unfortunately, direct measurements of the water table depth at Borden Forest are unavailable. However, groundwater data from nearby piezometers indicate annual water table fluctuations ranging from 0.25 m to 5.7 m below the surface.

The rooting depths of the major tree species at Borden Forest were also examined to evaluate to what extent the calculated effective soil moisture depth is consistent with other soil hydrology and vegetation properties at the site. Table 4 summarizes the varying rooting depths of the forest's common tree species, which include Red Maple, Large-tooth Aspen, White Ash, and White Pine.

Table 4: Rooting depth of the most common tree species in the Borden Forest.

Species	**Rooting depth**
Red Maple	11 cm to 174 cm
Large-tooth Aspen	Maximum 30 cm
White Ash	Can extend several meters
White Pine	Can extend several meters

With an estimated median effective soil moisture concentrated around a depth of 162 cm, this SM reservoir is likely accessible to deep-rooted species like Red Maple, White Ash, and White Pine. Shallow-rooted species, such as Large-tooth Aspen, with a maximum rooting depth of ~30 cm, often do not have access to deeper moisture. Given the wide range of water table depths reported in the surrounding areas (0.25 to 5.7 m), the estimated effective soil moisture depth of ~162 cm is also consistent with the presence of groundwater or a stable, deeper SM reservoir (Canadell et al., 1996; Schenk and Jackson, 2002). Thus, deeper soil layers are likely to play a significant role in regulating stomatal conductance and, consequently, ozone uptake at the Borden Forest site. Nonetheless, on-site water-table measurements and direct observations of rooting distributions would be essential to further confirm these findings.

4.4. Evaluating default and modified model outputs against measured V_{dO3}

Following the derivation of the effective soil moisture values in previous section, we ran two MLC-CHEM simulations to assess how well the model captures ozone deposition velocity when different SM inputs are used. Only the effective soil moisture values derived from deeper soil properties were used, as they were considered more likely to represent actual conditions. One simulation employs the default SM dataset at 50 cm depth (hereafter called SM_{50}), which follows the AQMEII convention of prescribing a maximum soil moisture of 0.24 m^3 m^{-3}. The other simulation (SM_{eff}) uses the inferred effective SM to represent a deeper effective rooting zone. These simulations were filtered out for any days where no valid inferred soil moisture data were available.

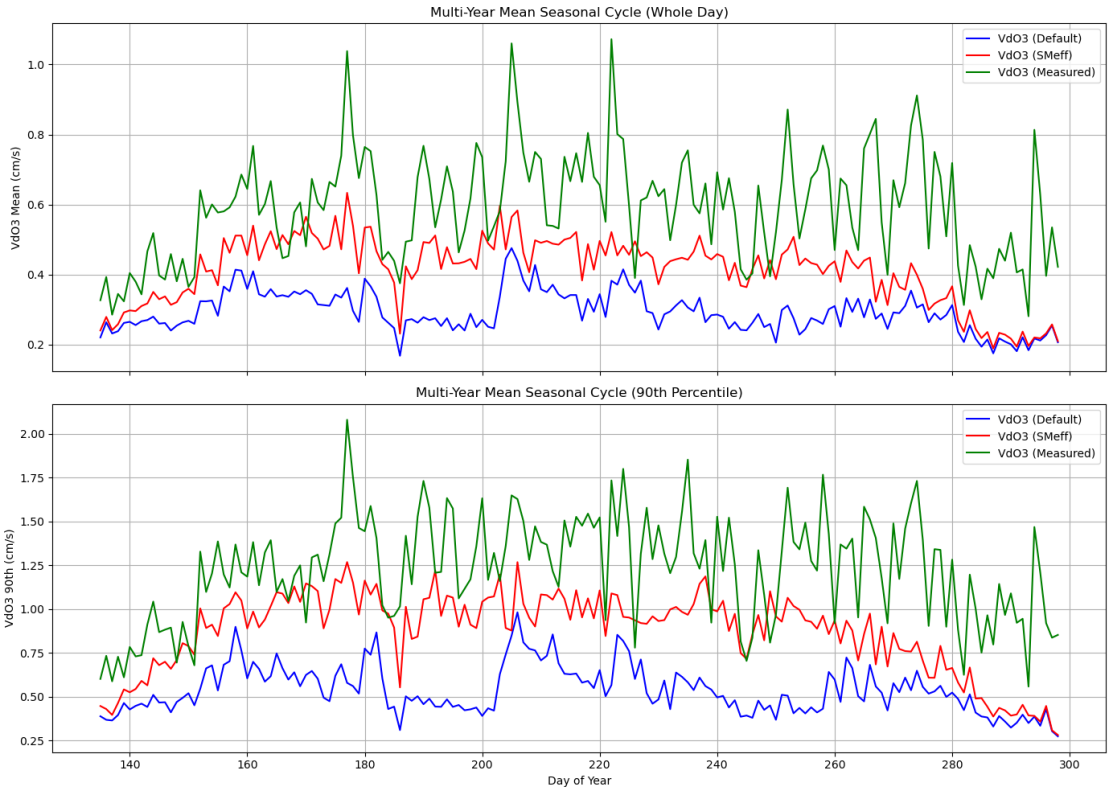

Figure 7: Comparison of the multi-year mean seasonal cycle (top panel) and 90th-percentile extremes (bottom panel) in measured V_{dO3} (green) versus model simulations using the default soil moisture (blue) and the inferred deeper soil moisture (red).

Figure 7 (top panel) compares the multi-year mean daily (or diurnal??) average of V_{dO3} from the default simulation (blue), the SM_{eff} simulation (red), and the measured (green) V_{dO3} values. Overall, the SM_{eff} simulation lies closer to the measured values than does the Default simulation. This improvement in modeled V_{dO3} magnitude is especially visible during the mid- to late-summer period (day of year ~150–250), suggesting that the deeper SM provides a more realistic water supply and thus higher stomatal uptake of ozone compared to the default shallower-moisture assumptions.

In the 90th percentile time series (Figure 7, bottom panel), representing peak or extreme events, the SM_{eff} run also shows higher values than the default simulation. Although this narrows the gap between model and observations, we still see that SM_{eff} simulation does not fully capture the large observed extremes in V_{dO3}. These short-term spikes occur on timescales shorter than would be expected from changes in SM alone, pointing to additional drivers of stomatal and non-stomatal removal of O_3 (e.g., increased canopy wetness or rapid chemical reactions with BVOCs) that are not fully represented in the current setup.

To quantify the improvements introduced by applying SM_{eff} instead of SM_{50}, a brief statistical analysis was conducted. As summarized in table 5, the SM_{eff} simulation improved the magnitude of V_{dO3} predictions by 32.6% (RMSE) and 38.3% (MAE) compared to the default simulation. Similarly, Table 8 shows that the improvement of predicting the interannual variability was increased by 14.1% (RMSE) and 17.7% (MAE) in the SM_{eff} simulation. However, the V_{dO3} remain underestimated, suggesting that non-stomatal removal mechanisms need additional consideration.

Table 5: Improvement in magnitude of ozone deposition velocity (V_{dO3}) predictions (SM_{eff} vs. Default).

Metric	Default	Wet	Improvement (%)
RMSE	0.323	0.218	32.6
MAE	0.296	0. 183	38.3

Table 6: Improvement in interannual variability of V_{dO3} predictions (SM_{eff} vs. Default).

Metric	Default	Wet	Improvement (%)
RMSE	0.191	0.164	14.1
MAE	0.158	0.130	17.7

4.5. Differences from measured V_{dO3} and meteorological drivers

To investigate model biases in more detail, the difference between the observed V_{dO3} and the SM_{eff} simulation results were plotted in Figure 8. The difference is predominantly positive over most days, which indicates that the improved SM_{eff} simulation tends to underestimate the measured V_{dO3}. Then the possible connection between these differences and meteorological variables, specifically, precipitation, relative humidity, temperature, and wind direction were explored.

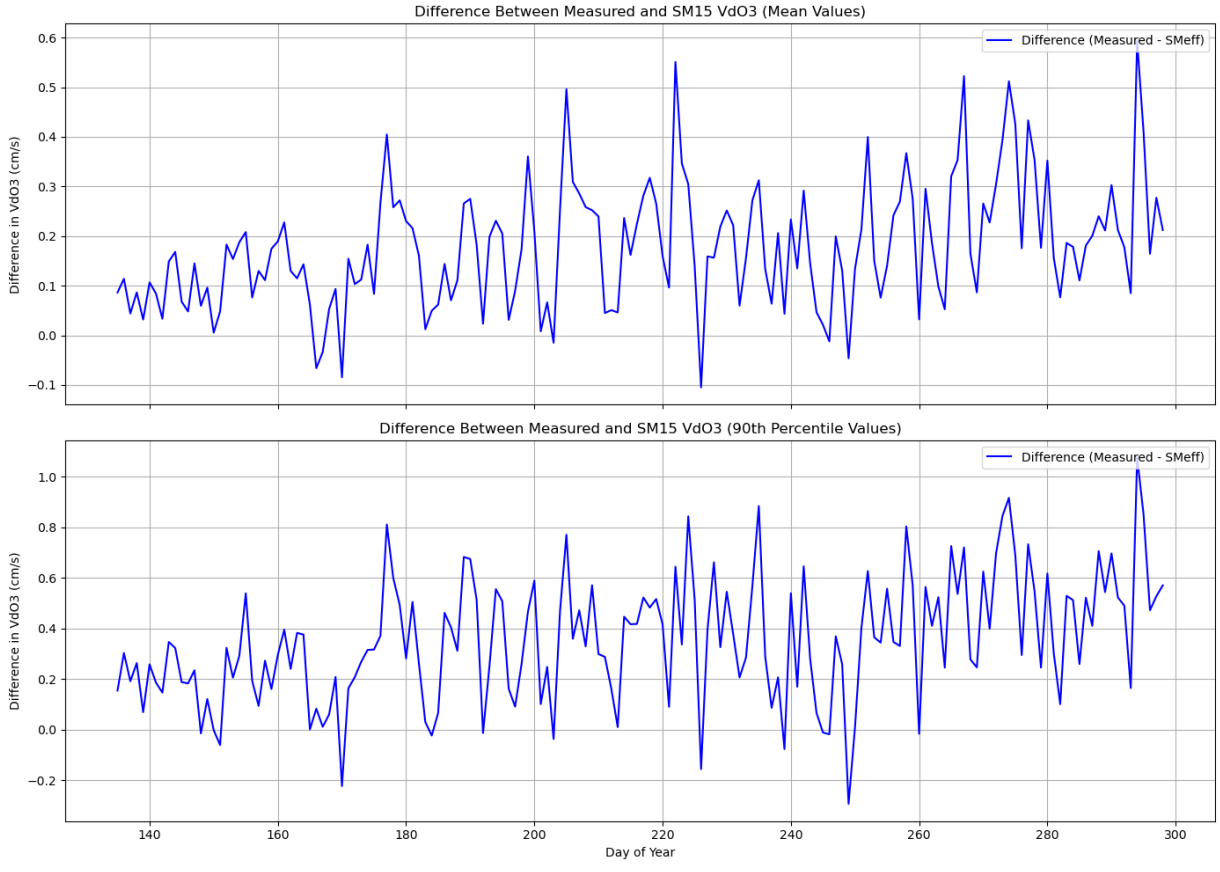

Figure 8: Time series of the difference between measured V_{dO3} and the SM_{eff} (modified deeper-soil) model simulation (top panel) and 90th-percentile extremes (bottom panel).

Figure 9 presents the relative effect of each variable on the V_{dO3} difference using absolute standardized coefficients. For both daytime and nighttime conditions, relative humidity appears as the strongest driver, followed by temperature, wind direction, and precipitation for daytime conditions, and wind direction, temperature, and precipitation for nighttime conditions.

To determine whether the model generally underestimates V_{dO3} values when RH is high, a regression analysis of the differences (Measured – SM_{eff}) was conducted. The results confirm a positive slope of approximately 0.86 ($R^2 \approx 0.10$, $p < 10^{-252}$), indicating that as RH increases, the underestimation of V_{dO3} grows. At RH ≥ 0.90, the mean difference is +0.305 cm s^{-1}, compared to +0.154 cm s^{-1} at RH < 0.90, which further supports the idea that at higher humidity, the model does not capture well the observed deposition velocities.

Physically, these findings are hinting at the role of canopy wetness and non-stomatal processes in increasing ozone uptake. At higher RH, leaf surfaces may remain moist or enable dew formation, as a result stimulating additional O_3 removal that is not exclusively stomatal. Although the SM_{eff} simulation better represents soil moisture limitations on stomata, it does not fully account for rapid changes in leaf wetness or dew formation, which can substantially increase observed V_{dO3}.

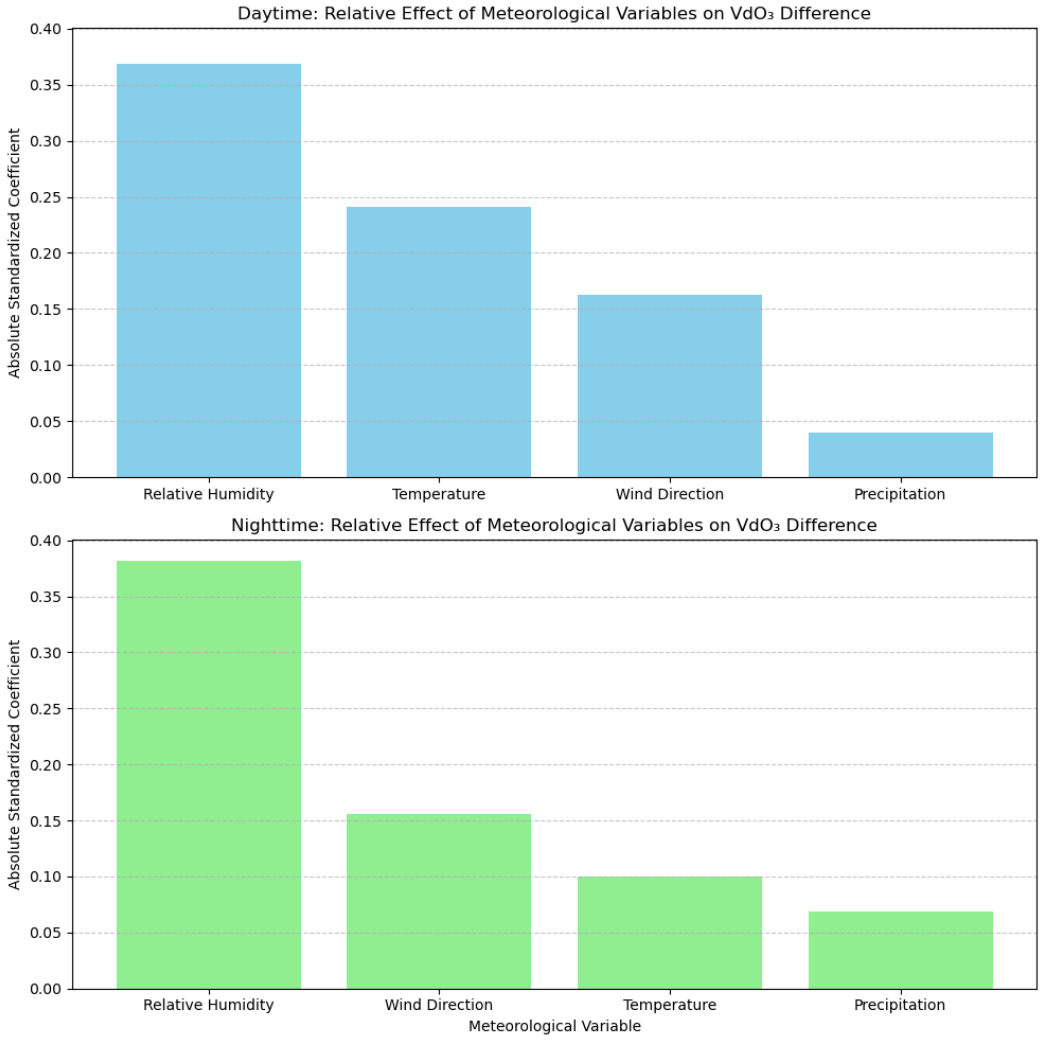

Figure 9: Relative influence of meteorological variables on the difference between measured and modeled V_{dO3} (SM_{eff}) for daytime conditions (top panel) and nighttime conditions (bottom panel), based on absolute standardized coefficients.

To further investigate the effect of canopy wetness on ozone deposition velocity, a new model simulation (hereafter referred to as Wet) with enhanced removal by the wet vegetation fraction was conducted, where the wet surface uptake resistance was reduced from from its default value of 2000 s/m in MLC-CHEM to 750 s/m.

The black line in Figure 10 represents the V_{dO3} values from the wet simulation. It is clear that with the enhanced wet removal, the wet simulation outperforms the SM_{eff} simulation in terms of magnitude and interannual variability.

To evaluate this improvement, a small statistical analysis was performed. Tables 7 and 8 show the results of this analysis. Compared to the SM_{eff} simulation, the Wet simulation significantly reduces both RMSE and MAE, with improvements of 34.3% and 38.9%, respectively, as shown in Table 7. Table 8 shows an improvement in interannual variability, with the wet simulation outperforming SM_{eff} but with smaller improvements. The Wet simulation provides a more consistent representation of interannual trends, as indicated by improvements in RMSE and MAE of 8.1% and 9.3%, respectively. These data suggest that canopy wetness may be the primary mechanism for non-stomatal O_3 uptake in the Borden Forest. But despite these improvements, peak ozone deposition velocities still remain underestimates suggesting that additional non-stomatal removal mechanism need to be explored in detail.

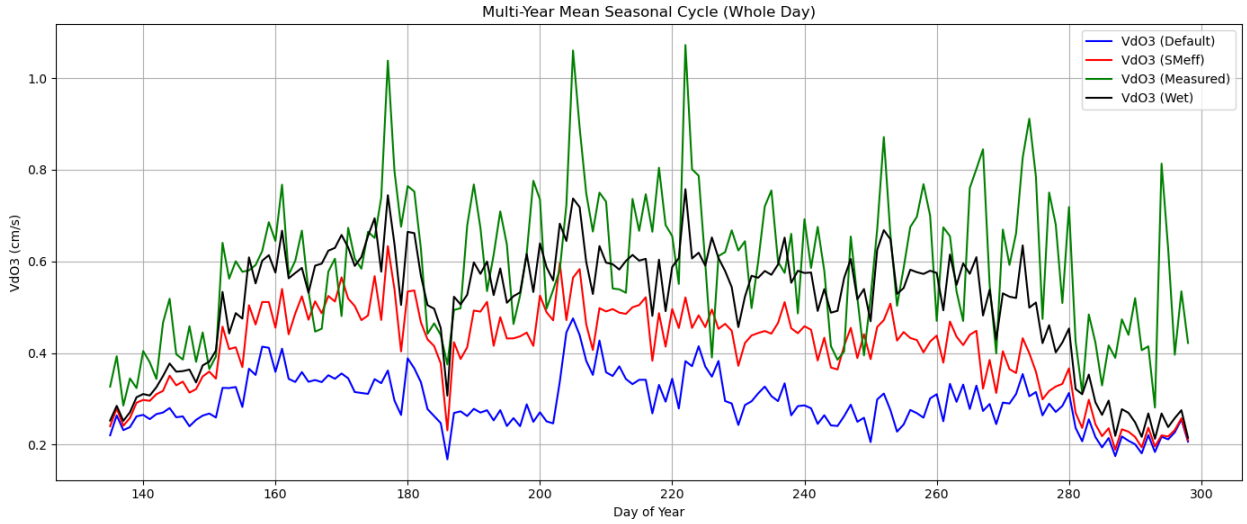

Figure 10: Multi-year mean seasonal cycle in measured V_{dO3} (green) versus model simulations using the default soil moisture (blue), inferred deeper soil moisture (red) and enhanced wet removal (black).

Table 7: Improvement in the magnitude of V_{dO3}predictions (SM_{eff} vs. Wet).

Metric	SM_{eff}	Wet	Improvement (%)
RMSE	0.218	0.143	34.3
MAE	0.183	0.111	38.9

Table 8: Improvement in the interannual variability of V_{dO3} predictions (SM_{eff} vs. Wet).

Metric	SM_{eff}	Wet	Improvement (%)
RMSE	0.164	0.151	8.1
MAE	0.130	0.118	9.3

5. Discussion

The following section discusses the key findings of this study, highlighting the implications of SM dynamics on ozone uptake processes. It examines the sensitivity of SM attenuation functions, the

role of depth-dependent SM in regulating plant water uptake, and the influence of non-stomatal ozone fluxes.

5.1. Selecting most suitable soil moisture attenuation function

As mentioned in Section 3.4, effective soil moisture values were initially averaged across multiple F_{ws} functions to provide a generalized representation of soil moisture stress impacts. Here, however given the large sensitivity of g_s and V_{dO3} to the representation of SM limitation, it is valuable to assess differences between the selected F_{ws} functions and how these differences might influence the interpretation of stomatal conductance and ozone deposition data. Four distinct functions were examined: the baseline polynomial (described in Section 3.4), along with cubic, logarithmic, and higher-order polynomial functions detailed in the Appendix. Figure 11 highlights the distinct shape and transition points of each function, illustrating how variations in the rate at which plants transition from low-stress to high-stress states can significantly affect model outputs under varying SM conditions. Understanding these variations is crucial for interpreting model sensitivity and reliability (Arora, 2002).

Among the examined SM stress functions, the cubic one ($F_{ws,cub}$) indicated by the green triangles introduces a steep transition near its critical moisture threshold, potentially increasing stress responses as the soil dries. In contrast, the logarithmic SM stress function ($F_{ws,log}$, blue diamonds) yields a more gradual transition, which could underrepresent severe drought stress. The higher order polynomial function ($F_{ws,p3}$, yellow crosses) provides an intermediate stress progression but still emphasizes stress more strongly than simpler linear formulations. Meanwhile, the baseline or "initial" polynomial function indicated by the red squares often used in simpler models strikes a balance between smooth and abrupt transitions (Verhoef & Egea, 2014). The diverse curves can affect both the timing of stomatal closure and ecosystem functions, including photosynthesis, transpiration rates, and gas fluxes like as ozone, especially when SM falls below critical thresholds (Fatichi et al., 2012).

Determining the most suitable F_{ws} function for a given application is challenging since each of the functions has its own set of advantages and disadvantages. In practice, choosing an optimal F_{ws} function is determined by how well this function can reflect local soil hydrological properties, plant root distribution and depth, and dominant climatic conditions (e.g., temperature, precipitation patterns, and evaporation rates) (Feddes et al., 1978; Clifton et al., 2021). For instance, a function that correctly simulates water retention in clay-rich soils may be useful in wet places, whereas a formula developed for sandy soils may work better in drier environments. Tailoring F_{ws} to site-specific conditions through in situ measurements, calibration against observed SM profiles, and validation with independent datasets can greatly improve model reliability and prediction accuracy (Rothfuss & Javaux, 2017). Although such customization was not performed in this study due to time constraints and other priorities, the potential for more realistic and reliable modeling of soil–plant interactions justifies further investment in this approach. This study has shown how such further studies can also benefit from inclusion of ozone flux measurements providing an additional constraint on stomatal conductance and the role of soil moisture limitation.

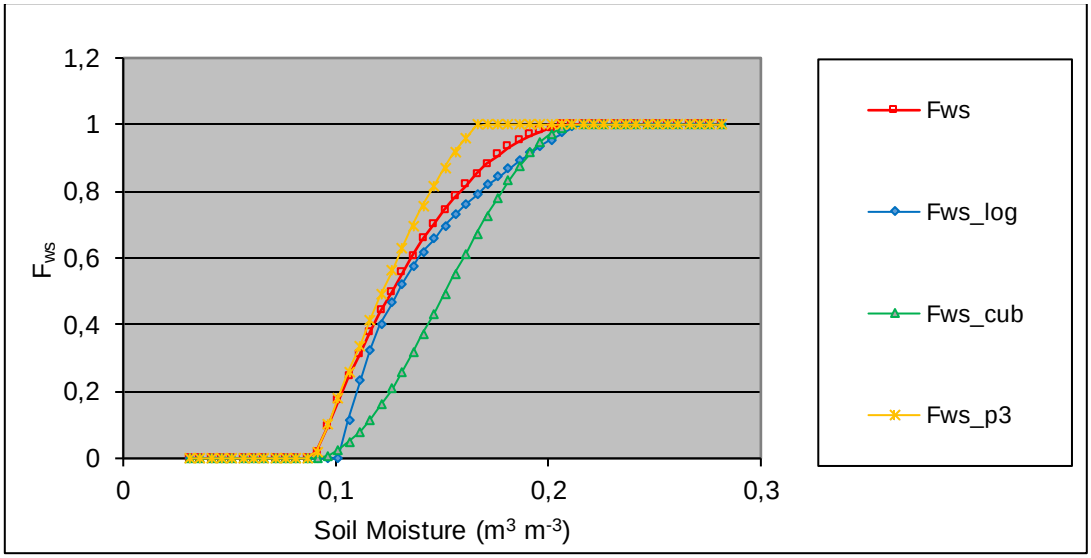

Figure 11: Comparison of four soil moisture attenuation functions across a range of soil moisture values. Each curve represents a distinct function: baseline polynomial (F_{ws}, red squares), logarithmic ($F_{ws,log}$, blue diamonds), cubic ($F_{ws,cub}$, green triangles), and a higher-order polynomial ($F_{ws,p3}$, yellow crosses).

5.2. Impact of soil moisture depth

This study emphasizes the need of considering integrated moisture content throughout many soil layers rather of relying solely on SM at the surface layer. This technique is consistent with the findings of Clifton et al. (2021) and Visser et al. (2022), who found that when simulating stomatal control and ozone deposition, multi-layer canopy exchange models such as MLC-CHEM benefit from integrating vertical SM profiles. According to Arora (2002) and Fatichi et al. (2012), deeper soil layers in some forest soils (such as Borden Forest) can actually store water and reduce surface deficits.

Plants in many forest settings can access deeper water reservoirs via root systems that extend far below the topsoil (Jackson et al., 2000) and where most of the soil moisture monitoring is conducted. Under mild to moderate drought conditions, Clifton and Visser (2023) found that including these subsurface moisture sources in MLC-CHEM reduced the discrepancies between predicted and observed fluxes. Cammalleri et al. (2020) found that underground water reserves can buffer plants from surface layer drought by delaying stomatal closure and maintaining photosynthetic activity. Drought stress may be overestimated by conventional SM attenuation functions that make the assumption of a single, constant root zone moisture level. Extending functions like the Feddes approach (Feddes et al., 1978) to stratify moisture by depth can yield more realistic plant water uptake profiles, as recommended by Clifton et al. (2021).

Using deeper SM improves g_s predictions while also allowing for the prediction of threshold reactions to dryness, particularly the point at which stomata close. According to Visser et al. (2021), multi-layer soil moisture inputs reduce uncertainty in drought related processes, highlighting the importance of detailed root zone parameterization for future modeling projects. However, the wide range of soil properties, like different water retention profiles which result from spatial variations in texture, porosity, and organic matter concentration, adds to the complexity (Rothfuss & Javaux, 2017). As a result, a simple linear or polynomial function F_{ws} may not reflect the full spectrum of plant responses in different soil layers. According to Fatichi & Pappas (2017), in situ moisture measurements at different depths can help adjust these functions accordingly. Nevertheless, Clifton and Visser (2023) highlight that such data-driven models must be carefully

validated against independent datasets to minimize overfitting and maintain consistent performance across a range of different environmental conditions.

5.3. Non-stomatal ozone uptake

This analysis shows that while adjustments to deeper soil moisture inputs (via the SM_{eff} simulation) have improved the simulation of stomatal uptake, the model continues to underestimate ozone deposition velocity, especially during periods with high surface-level moisture resulting in high stomatal uptake rates. However, also for these conditions non-stomatal pathways still play a crucial role during nocturnal stomatal closure.

Analysis of the data shows a significant increase in the discrepancy between predicted and actual ozone deposition rates when relative humidity exceeds 90%. This gap can be partially explained by increasing effect of canopy wetness. Long-term leaf wetness, along with moisture on the bark and forest floor, creates a continuous water layer under these humid conditions, increasing the reactive surface available for ozone uptake. However, as Clifton et al. (2023) note, our current parameterizations may be missing important processes and interconnections, particularly given that ozone is only sparingly soluble in water (Seinfeld & Pandis, 2016), which limits the extent to which aqueous films can serve as an effective medium for ozone uptake. Furthermore, rapid dew formation and evaporation can cause short-term bursts of ozone removal over much shorter time periods than changes in SM, highlighting an important gap in current modeling.

In addition to the physical effects of canopy wetness, it is important to consider the role of biogenic volatile organic compounds (BVOCs) in ozone removal. Forest canopies release BVOCs, such as isoprene and other mono- and higher terpenes, of which some react quickly with ozone. These processes may not only directly contribute to ozone removal, but also produce secondary organic aerosols, which alter the reactive capacity of canopy surfaces (Anav et al., 2018; Zhou et al., 2017). Nonetheless, the efficient O_3 uptake observed at high relative humidity is more compatible with direct physical processes, such as increased leaf moisture, than with BVOC responses. Furthermore, temperate forests as present at the Borden site often have low BVOC emission rates (Atkinson, 2000; Guenther et al., 2012; Kesselmeier & Staudt, 1999), implying that BVOC-driven chemistry is unlikely to be the major non-stomatal mechanism here.

Additionally, recent findings highlight the role of soil nitric oxide (NO) emissions in contributing to ozone deposition. Under certain conditions, NO emitted from the soil can rapidly react with ozone in the near-surface layer, increasing apparent ozone uptake rates. This mechanism was shown to be particularly relevant at the Bosca Fontana site, where large soil NO emissions explained a large fraction of the observed O_3 removal (Visser et al., 2022). Although soil NO emissions at Borden Forest are expected to be lower than those at intensively managed or fertilized sites, this pathway may still contribute to non-stomatal ozone fluxes and requires further consideration.

To represent moisture-driven processes, model improvements must go beyond SM and stomatal conductance alone. Integrating high-resolution canopy moisture measurements, in particular continuous leaf wetness data, which were unavailable at Borden Forest, with sophisticated high-frequency ozone flux observations could aid in understanding short-term dew formation and evaporation dynamics. Additionally, improving the chemical kinetics associated with BVOC reactivity, especially in the presence of water films, will be critical to properly simulate non-stomatal ozone uptake in models such as MLC-CHEM (Clifton et al., 2023). These efforts could narrow the gap between modeled and observed V_{dO3} levels by considering the interactions between canopy wetness and in-canopy chemical processes.

6. Conclusion

This study provides new insides on the function of soil moisture in both stomatal and non-stomatal ozone uptake throughout seasons. Using the Multilayer Canopy and Chemical Exchange Model (MLC-CHEM) and long-term ozone flux measurements from the Borden Forest, this study confirmed that SM plays a crucial role in regulating ozone deposition velocity. These results emphasize the need of considering SM at deeper depths than it is actually measured, as stomatal conductance is regulated by water availability at depths much deeper than the depths of soil moisture measurements.

Comparison of soil moisture values at 2 cm and 50 cm depths showed that the deeper soil layers provided plants with a more stable water supply, which in turn improved stomatal conductance values. However, even at 50 cm depth, discrepancies between observed and inferred stomatal conductance suggest that the true limiting SM depth is even deeper. Through the derivation of an effective soil moisture depth, estimated to concentrated around a depth of approximately 162 cm, this study emphasizes the necessity of considering subsurface moisture reserves when evaluating plant water availability and its effect on ozone uptake.

MLC-CHEM modeling experiments indicate that incorporating deeper SM (SM_{eff} simulation) significantly improves the simulated ozone deposition velocity, especially during mid- to late-summer when moisture stress is most pronounced. Specifically, the SM_{eff} simulation reduced prediction errors by approximately 32.6–38.3% in magnitude and by 14.1–17.7% in interannual variability compared to the default simulation. However, even with these improvements, the model still underestimates V_{dO3} under high relative humidity conditions. New simulation findings that include increased wet removal, a proxy for canopy wetness effects, further reduced errors in magnitude by an additional 34.3–38.9% and interannual variability by 8.1–9.3%. These data show that, in addition to deeper soil moisture inputs, non-stomatal processes driven primarily by canopy wetness play a significant role in ozone absorption under humid conditions.

These findings have wide-ranging consequences for modeling vegetation-atmosphere interactions, climate feedback mechanisms, and air quality. The study emphasizes the relevance of deep SM measurements in forest ecosystems as well as the limits of existing models that rely solely on surface or shallow moisture data. Moreover, the results also imply that high-resolution canopy moisture and atmospheric chemistry data are needed to fully understand the complex processes that control ozone uptake including the partitioning between stomatal and non-stomatal uptake mechanisms.

Future research should focus on integrating continuous leaf wetness measurements and improving the representation of non-stomatal processes in air quality models, including the effects of canopy wetness and biogenic volatile organic compound (BVOC) and NO emissions on ozone deposition. Furthermore, regional variability in soil moisture and root water uptake in different forest ecosystems should be studied in order to improve the accuracy of ozone deposition model predictions. By addressing these gaps, researchers can improve the ability of atmospheric models to simulate ozone fluxes and estimates of ecosystem responses to changing climate conditions.

References

Kampa, M., & Castanas, E. (2008). Human health effects of air pollution. Environmental Pollution, 151(2), 362–367. https://doi.org/10.1016/j.envpol.2007.06.012

Change, N. I. P. O. C. (2023). Climate Change 2021 – The Physical science basis. https://doi.org/10.1017/9781009157896

Monks, P. S. (2005). Gas-phase radical chemistry in the troposphere. Chemical Society Reviews, 34(5), 376. https://doi.org/10.1039/b307982c

Ashmore, M. R. (2005). Assessing the future global impacts of ozone on vegetation. Plant Cell & Environment, 28(8), 949–964. https://doi.org/10.1111/j.1365-3040.2005.01341.x

Zhou, P., Ganzeveld, L., Rannik, Ü., Zhou, L., Gierens, R., Taipale, D., Mammarella, I., & Boy, M. (2017). Simulating ozone dry deposition at a boreal forest with a multi-layer canopy deposition model. Atmospheric Chemistry and Physics, 17(2), 1361–1379. https://doi.org/10.5194/acp-17-1361-2017

Clifton, O. E., Schwede, D., Hogrefe, C., Bash, J. O., Bland, S., Cheung, P., Coyle, M., Emberson, L., Flemming, J., Fredj, E., Galmarini, S., Ganzeveld, L., Gazetas, O., Goded, I., Holmes, C. D., Horváth, L., Huijnen, V., Li, Q., Makar, P. A., . . . Zhang, L. (2023). A single-point modeling approach for the intercomparison and evaluation of ozone dry deposition across chemical transport models (Activity 2 of AQMEII4). Atmospheric Chemistry and Physics, 23(17), 9911–9961. https://doi.org/10.5194/acp-23-9911-2023

Visser, A. J., Ganzeveld, L. N., Goded, I., Krol, M. C., Mammarella, I., Manca, G., & Boersma, K. F. (2021). Ozone deposition impact assessments for forest canopies require accurate ozone flux partitioning on diurnal timescales. Atmospheric Chemistry and Physics, 21(24), 18393–18411. https://doi.org/10.5194/acp-21-18393-2021

Anav, A., Proietti, C., Menut, L., Carnicelli, S., De Marco, A., & Paoletti, E. (2018). Sensitivity of stomatal conductance to soil moisture: implications for tropospheric ozone. Atmospheric Chemistry and Physics, 18(8), 5747–5763. https://doi.org/10.5194/acp-18-5747-2018

Khan, A. M., Clifton, O. E., Bash, J. O., Bland, S., Booth, N., Cheung, P., Emberson, L., Flemming, J., Fredj, E., Galmarini, S., Ganzeveld, L., Gazetas, O., Goded, I., Hogrefe, C., Holmes, C. D., Horvath, L., Huijnen, V., Li, Q., Makar, P. A., . . . Stoy, P. C. (2024). Ozone dry deposition through plant stomata: Multi-model comparison with flux observations and the role of water stress as part of AQMEII4 Activity 2. EGUsphere. https://doi.org/10.5194/egusphere-2024-3038

Davison, A. W., & Barnes, J. D. (1998). Effects of ozone on wild plants. New Phytologist, 139(1), 135–151. https://doi.org/10.1046/j.1469-8137.1998.00177.x

Visser, A. J., Ganzeveld, L. N., Finco, A., Krol, M. C., Marzuoli, R., & Boersma, K. F. (2022). The combined impact of canopy stability and soil NOx exchange on ozone removal in a temperate deciduous forest. Journal of Geophysical Research Biogeosciences, 127(10). https://doi.org/10.1029/2022jg006997

Clifton, O. E., Fiore, A. M., Massman, W. J., Baublitz, C. B., Coyle, M., Emberson, L., Fares, S., Farmer, D. K., Gentine, P., Gerosa, G., Guenther, A. B., Helmig, D., Lombardozzi, D. L., Munger, J. W., Patton, E. G., Pusede, S. E., Schwede, D. B., Silva, S. J., Sörgel, M., . . . Tai, A. P. K. (2020). Dry deposition of ozone over land: processes, measurement, and modeling. Reviews of Geophysics, 58(1). https://doi.org/10.1029/2019rg000670

Altimir, N., Kolari, P., Tuovinen, J., Vesala, T., Bäck, J., Suni, T., Kulmala, M., & Hari, P. (2006). Foliage surface ozone deposition: a role for surface moisture? Biogeosciences, 3(2), 209–228. https://doi.org/10.5194/bg-3-209-2006

Rao, S. T., Galmarini, S., & Puckett, K. (2010). Air Quality Model Evaluation International Initiative (AQMEII): Advancing the state of the science in regional photochemical modeling and its applications. Bulletin of the American Meteorological Society, 92(1), 23–30. https://doi.org/10.1175/2010bams3069.1

Jarvis, P. G. (1976). The interpretation of the variations in leaf water potential and stomatal conductance found in canopies in the field. Philosophical Transactions of the Royal Society of

London. Series B, Biological Sciences, 273(927), 593–610. https://doi.org/10.1098/rstb.1976.0035

Zettl, J. D., et al. (2011). Soil texture and moisture retention relationships. Geoderma, 160(3-4), 345-355.

Famiglietti, J. S., & Wood, E. F. (1994). Multiscale modeling of spatially variable water and energy balance processes. Water Resources Research, 30(11), 3061-3078.

Baldocchi, D. D., et al. (2004). Measuring and modeling ecosystem carbon exchange in response to seasonal and interannual variations in soil moisture. *Agricultural and Forest Meteorology*, 123(1-2), 13-39.

Lawrence, D. M., & Slater, A. G. (2008). Incorporating organic soil into a global climate model. *Climate Dynamics*, 30(2-3), 145-160.

Porporato, A., Laio, F., Ridolfi, L., & Rodriguez-Iturbe, I. (2001). Plants in water-controlled ecosystems: active role in hydrologic processes and response to water stress. Advances in Water Resources, 24(7), 725–744. https://doi.org/10.1016/s0309-1708(01)00006-9

Landsberg, J., & Waring, R. (1997). A generalised model of forest productivity using simplified concepts of radiation-use efficiency, carbon balance and partitioning. Forest Ecology and Management, 95(3), 209–228. https://doi.org/10.1016/s0378-1127(97)00026-1

Granier, A., Reichstein, M., Bréda, N., Janssens, I., Falge, E., Ciais, P., Grünwald, T., Aubinet, M., Berbigier, P., Bernhofer, C., Buchmann, N., Facini, O., Grassi, G., Heinesch, B., Ilvesniemi, H., Keronen, P., Knohl, A., Köstner, B., Lagergren, F., . . . Wang, Q. (2007). Evidence for soil water control on carbon and water dynamics in European forests during the extremely dry year: 2003. Agricultural and Forest Meteorology, 143(1–2), 123–145. https://doi.org/10.1016/j.agrformet.2006.12.004

Hillel, D. (2004). *Introduction to environmental soil physics* (2nd ed.). Academic Press.

Jarvis, P. G., & McNaughton, K. G. (1986). Stomatal control of transpiration: Scaling up from leaf to region. Advances in Ecological Research, 15, 1–49. https://doi.org/10.1016/S0065-2504(08)60119-1

Oishi, A. C., Oren, R., & Stoy, P. C. (2008). Estimating components of forest evapotranspiration: A footprint approach for scaling sap flux measurements. Agricultural and Forest Meteorology, 148(11), 1719–1732. https://doi.org/10.1016/j.agrformet.2008.06.013

Bréda, N., Granier, A., & Aussenac, G. (1995). Effects of thinning on soil and tree water relations, transpiration and growth in an oak forest (Quercus petraea (Matt.) Liebl.). Tree Physiology, 15(5), 295–306. https://doi.org/10.1093/treephys/15.5.295

Damour, G., Simonneau, T., Cochard, H., & Urban, L. (2010). An overview of models of stomatal conductance at the leaf level. Plant, Cell & Environment, 33(9), 1419–1438. https://doi.org/10.1111/j.1365-3040.2010.02181.x

Monteith, J. L., & Unsworth, M. H. (2008). Principles of Environmental Physics. Academic Press.

Pataki, D. E., & Oren, R. (2003). Species differences in stomatal control of water loss at the canopy scale in a mature bottomland deciduous forest. Advances in Water Resources, 26(12), 1267–1278. https://doi.org/10.1016/j.advwatres.2003.08.002

Van Genuchten, M. T. (1980). A closed-form equation for predicting the hydraulic conductivity of unsaturated soils. Soil Science Society of America Journal, 44(5), 892–898. https://doi.org/10.2136/sssaj1980.03615995004400050002x

Dickinson, E., Henderson-Sellers, A., Kennedy, J., & Wilson, F. (1986b). Biosphere-Atmosphere Transfer Scheme (BATS) for the NCAR Community climate model. CTIT Technical Reports Series. https://doi.org/10.5065/d6668b58

Dane, Jacob & Topp, Clarke & Romano, Nunzio & Santini, Alessandro. (2002). 3.3.3 Field. 10.2136/sssabookser5.4.c26.

Canadell, J., Jackson, R. B., Ehleringer, J. B., Mooney, H. A., Sala, O. E., & Schulze, E. (1996). Maximum rooting depth of vegetation types at the global scale. Oecologia, 108(4), 583–595. https://doi.org/10.1007/bf00329030

Schenk, H. J., & Jackson, R. B. (2002). Rooting depths, lateral root spreads and below-ground/above-ground allometries of plants in water-limited ecosystems. Journal of Ecology, 90(3), 480–494. https://doi.org/10.1046/j.1365-2745.2002.00682.x

Arora, V. (2002). Modeling vegetation as a dynamic component in soil-vegetation-atmosphere transfer schemes and hydrological models. Reviews of Geophysics, 40(2). https://doi.org/10.1029/2001rg000103

Fatichi, S., Pappas, C., & Ivanov, V. Y. (2015). Modeling plant–water interactions: an ecohydrological overview from the cell to the global scale. Wiley Interdisciplinary Reviews Water, 3(3), 327–368. https://doi.org/10.1002/wat2.1125

Feddes, R. A., Kowalik, P. J., & Zaradny, H. (1978). Simulation of field water use and crop yield. http://ci.nii.ac.jp/ncid/BA07819710

Rothfuss, Y., & Javaux, M. (2017). Reviews and syntheses: Isotopic approaches to quantify root water uptake: a review and comparison of methods. Biogeosciences, 14(8), 2199–2224. https://doi.org/10.5194/bg-14-2199-2017

Verhoef, A., & Egea, G. (2014). Modeling plant transpiration under limited soil water: Comparison of different plant and soil hydraulic parameterizations and preliminary implications for their use in land surface models. Agricultural and Forest Meteorology, 191, 22–32. https://doi.org/10.1016/j.agrformet.2014.02.009

Appendix

All soil moisture attenuation functions

Below presented all of the different F_{ws} functions that were used in this study. Baseline or initial polynomial function was presented in the methodology section.

Cubic formula:

$$F_{ws} = 3 \times \left(\frac{Ws-Wp}{Wcr-Wp}\right)^2 - 2 \times \left(\frac{Ws-Wp}{Wcr-Wp}\right)^3 \quad \text{(eq. 7)}$$

Logarithmic formula:

$$= 1 + \log\left(\frac{Ws-Wp}{Wcr-Wp}\right) \quad \text{(eq. 8)}$$

Polynomial formula:

$$F_{ws} = 2 \times \left(\frac{Ws-Wp}{Wcr-Wp}\right) - \left(\frac{Ws-Wp}{Wcr-Wp}\right)^3 \quad \text{(eq. 9)}$$

Effective soil moisture derivation

Below the process of determining inferred stomatal conductance ($g_{s,fws}$) is shown. By dividing $g_{s,obs}$ by $g_{s,opt}$, the F_{ws} can be calculated for each data point:

$$F_{ws} = \frac{g_{s,obs}}{g_{s,opt}} \quad \text{(eq. 10)}$$

Once the F_{ws} values are determined, the next step involves rearranging the F_{ws} function to solve for soil moisture.

To simplify, let:

$$x = \frac{Ws-Wp}{Wcr-Wp} \quad \text{(eq. 11)}$$

Substituting x into the F_{ws} equation results in the following:

$$F_{ws} = 2x - x^2 \quad \text{(eq. 12)}$$

Rearranging this equation leads to a standard quadratic form:

$$x^2 - 2x + F_{ws} = 0 \quad \text{(eq. 13)}$$

The quadratic formula is then applied to solve for x:

$$x = \frac{-b \pm \sqrt{b^2-4ac}}{2a} \quad \text{(eq. 14)}$$

In this case:

$$a = 1$$

$$b = -2$$

$$c = Fws$$

This results in:

$$x = \frac{2 \pm \sqrt{4-4\times F_{ws}}}{2} = 1 \pm \sqrt{1-F_{ws}} \quad \text{(eq. 15)}$$

Because x represents a fraction $\left(\frac{Ws-Wp}{Wcr-Wp}\right)$ that must fall between 0 and 1, the only valid solution is: $x = 1 - \sqrt{1-F_{ws}}$ (eq. 16)

Finally, the value of x is substituted back into the original equation for Ws to calculate the effective soil moisture:

$$Ws = Wp + x \times (Wcr - Wp) \quad \text{(eq. 17)}$$

Using this formula, effective soil moisture values are calculated for each data point. These effective values represent the soil moisture levels that correspond to the calculated F_{ws}.

Soil data necessary for the normalization

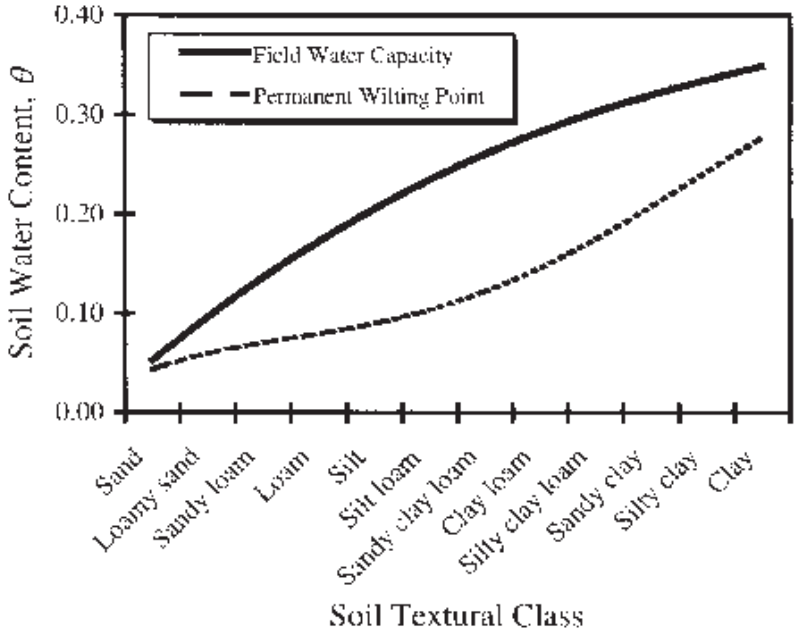

Figure 12: Soil water content represented by the soil texture class.

Figure 12 illustrates soil water content as represented by soil texture class, showing permanent wilting point and field capacity for various soil textures. In the study site, the topsoil exhibits different characteristics than the deeper layers (typically clay loam below 50 cm). By comparing the effective soil moisture with the values for clay loam (or other relevant soil types), we can infer whether the depth of the limiting soil moisture extends as far as the water table or remains above it.